



## Article

# Integrating Fermentation Engineering and Organopalladium Chemocatalysis for the Production of Squalene from Biomass-Derived Carbohydrates as the Starting Material

Cuicui Wu , Kaifei Tian, Xuan Guo \* and Yunming Fang \*

National Energy R&D Research Center for Biorefinery, Department of Chemical Engineering, Beijing University of Chemical Technology, Beijing 100029, China; wu941210@buct.edu.cn (C.W.); tiankfei@126.com (K.T.)

\* Correspondence: guoxuan19930426@163.com (X.G.); fangym@mail.buct.edu.cn (Y.F.)

**Abstract:** The transition from fossil resources to renewable biomass for the production of valuable chemicals and biobased fuels is a crucial step towards carbon neutrality. Squalene, a valuable chemical extensively used in the energy, healthcare, and pharmaceutical fields, has traditionally been isolated from the liver oils of deep-sea sharks and plant seed oils. In this study, a biochemical synergistic conversion strategy was designed and realized to convert glucose to squalene by combining fermentation technology in yeast with reductive coupling treatment of dienes. First, glucose derived from hydrolysis of cellulose was used as a renewable resource, using genetically engineered *Saccharomyces cerevisiae* as the initial biocatalyst to produce  $\beta$ -farnesene with a titer of 27.6 g/L in a 2.5 L bioreactor. Subsequently, intermediate  $\beta$ -farnesene was successfully converted to squalene through the organopalladium-catalyzed reductive coupling reaction involving the formation of Pd(0)L<sub>2</sub> species. Under mild reaction conditions, impressive  $\beta$ -farnesene conversion (99%) and squalene selectivity (100%) were achieved over the Pd(acac)<sub>2</sub> catalyst at a temperature of 75 °C in an ethanol solvent after 5 h. This advancement may provide insights into broadening squalene production channels and accessing the complex skeletons of natural terpenoids from biorenewable carbon sources, offering practical significance and economic benefits.



check for updates

**Citation:** Wu, C.; Tian, K.; Guo, X.; Fang, Y. Integrating Fermentation Engineering and Organopalladium Chemocatalysis for the Production of Squalene from Biomass-Derived Carbohydrates as the Starting Material. *Catalysts* **2023**, *13*, 1392. <https://doi.org/10.3390/catal13111392>

Academic Editors: Valeria La Parola and Leonarda Liotta

Received: 21 August 2023

Revised: 12 October 2023

Accepted: 19 October 2023

Published: 25 October 2023



**Copyright:** © 2023 by the authors. Licensee MDPI, Basel, Switzerland. This article is an open access article distributed under the terms and conditions of the Creative Commons Attribution (CC BY) license (<https://creativecommons.org/licenses/by/4.0/>).

**Keywords:** squalene;  $\beta$ -farnesene; fermentation technology; reductive coupling of dienes; *Saccharomyces cerevisiae*

## 1. Introduction

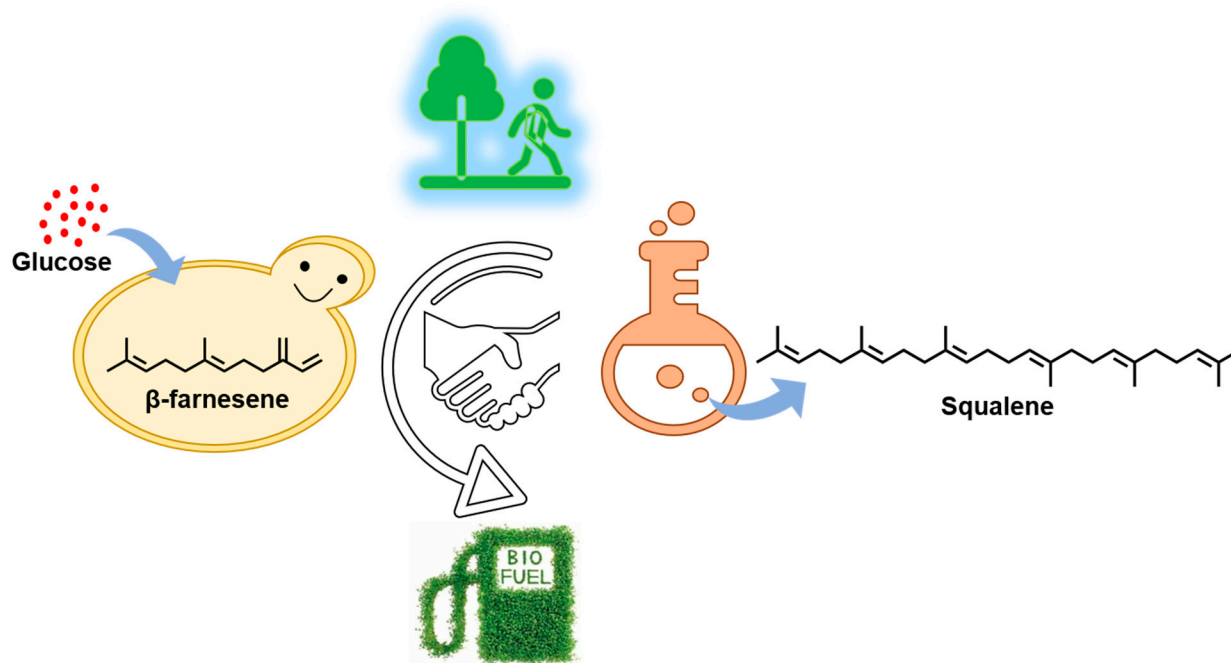
The increasing deterioration of the environment and the depletion of fossil resources have led to a search for environmentally friendly renewable chemicals and fuels to reduce dependence on petroleum-based energy [1–7]. Biorefineries that utilize sustainable biomass sugars offer significant opportunities for the production of liquid biofuels, which can serve as alternative fuels for transportation, thus addressing the global fuel energy crisis [8–12]. In this study, we explored the fermentation of biomass carbon sources coupled with chemical conversion to deliver full-performance fuel components, including  $\beta$ -farnesene and squalene, which could also be blended with conventional jet fuels. By obtaining a better understanding of their structure and function, these fuels may offer a significantly wider application range for platform intermediates through chemocatalytic upgrading [13–16].

Farnesene is a sesquiterpene composed of three isoprene units, consisting of  $\alpha$ - and  $\beta$ -isomers typically present in nature, though the  $\beta$ -isomer is more active toward polymerization and oligomerization [17–20]. Glucose can be used as a supplementary carbon source to obtain high-purity biobased  $\beta$ -farnesene under the action of microbial metabolic engineering [21]. Due to the presence of a conjugated double bond in its molecular structure,  $\beta$ -farnesene possesses various excellent properties which are applicable in the energy, agriculture, and food industries [22,23]. For example, Liu et al. reported for the first time on the two-stage biotransformation of waste cooking oils by engineering *Escherichia coli*

for the production of fatty acid methyl esters and  $\beta$ -farnesene, and  $\beta$ -farnesene has been recognized as a jet biofuel because of its unprecedented low-temperature performance and gravimetric heat of combustion [24]. Numerous studies have been conducted in recent years on production via exploiting the metabolic engineering of *S. cerevisiae* [25–32]. In 2016, Adam L. Meadows et al. fundamentally altered glycolysis and the production of central metabolites (cytosolic acetyl-CoA), further improving the ability of *S. cerevisiae* strains to produce  $\beta$ -farnesene [23].

Squalene is a chained triterpenoid compound with six isolated C=C bonds in a molecular framework, endowing it with unique properties useful in medical and industrial applications [33–40]. Many studies have shown that squalene can be used as an alternative high-quality transportation fuel, potentially replacing petroleum to capture the market share of hydrocarbon biofuels. Squalene can also serve as an alternative feedstock for petroleum-based products if produced commercially in a sustainable manner. However, restrictions on the hunting of deep-sea sharks have led to a sharp decline in the production of natural high-quality squalene [41–43]. The reductive coupling of dienes catalyzed by organopalladium can achieve carbon chain extension and form C–C or C–H bonds, and this reaction has been widely used in pharmaceutical synthesis, fine chemicals, alternative energy, and other fields [44–47]. Compared to heterogeneous catalysts, homogeneous catalysts generally possess well-defined structures, with optimized superior activity and/or selectivity under very mild reaction conditions, even at a low catalyst dosage [48–50]. For example, Yu et al. developed a reductive homocoupling of allylic acetates through cooperative palladium and photoredox catalysis, allowing for the construction of C(sp<sup>3</sup>)-C(sp<sup>3</sup>) bonds under mild reaction conditions, which easily prepared a series of C2-symmetrical chiral 1,5-dienes [51]. In the progression of our experimental practice, it was discovered that  $\beta$ -farnesene can be entirely converted into squalene using homologous coordination molecules of organic palladium and phosphine as the catalyst, at low-temperature, atmospheric-pressure conditions and using a small amount of catalyst. If mass-produced on an industrial scale, this innovative route could greatly increase the annual production of squalene and reduce the production cost.

In this work, we developed a feasible hybrid process for the production of high-performance sustainable aircraft fuel C30 squalene using biomass-derived carbohydrates as the starting material. The detailed process is presented in Scheme 1. In the first step, glucose as a carbon source was metabolized to biobased  $\beta$ -farnesene through microbial cell factories. In the second step,  $\beta$ -farnesene isolated from a bioreactor was dimerized into squalene as jet fuel blendstock for market militarization potential using commercial organometallic palladium complexes. A series of fermentation process arguments (initial glucose concentration, supplementary carbon sources, and substrate addition fermentation) and chemocatalysis reaction parameters (organopalladium catalysts, catalyst loading amount, PPh<sub>3</sub> amount, substance concentration, temperature, and solvents) were investigated through single factor control. Moreover, in order to better understand this reaction process, the transformation mechanism from  $\beta$ -farnesene to squalene was studied. This approach seamlessly combined the advantages of bacterial metabolism specificity and chemical catalysis efficiency, resulting in an ideal biofuel or conventional fuel additive. This approach demonstrated the potential for utilizing biomass resources and developing a synthetic pathway for high-value-added squalene.



**Scheme 1.** Route for producing squalene fuel with glucose through metabolic engineering merged with organopalladium chemocatalysis.

## 2. Results and Discussion

### 2.1. Establishment of the $\beta$ -Farnesene Fermentation Process

As exhibited in Scheme 1,  $\beta$ -farnesene was the most important functionalized intermediate for squalene tandem transformation, bridging the gap between bio- and chemo-catalysis. To obtain a large and neat squalene precursor, scaled-up fermentation of the genetically engineered *S. cerevisiae* as a  $\beta$ -farnesene producer was performed in a 2.5 L bioreactor. This bioprocessing process with different initial glucose concentrations was run to determine the initial glucose concentration in the medium, and the core strategy of sugar limitation and feeding. The biological influence cofactors of the initial glucose concentration, supplementary carbon sources, and substrate addition fermentation were optimized under mild performance conditions.

#### 2.1.1. Initial Glucose Concentration

The fermentation performance of initial glucose content, with three initial values of 20, 40, and 60 g/L, was investigated for a total fermentation time of 109 h. As represented in Figure 1a, the  $OD_{600}$  value was positively correlated with improvements in initial glucose concentration. In addition, we found that  $OD_{600}$  with 60 g/L of glucose rapidly reached 87 after 109 h of fermentation, indicating that increases in initial glucose concentration accelerated the proliferation and growth of the strain population [52]. As displayed in Figure 1b, 4.07 and 4.24 g/L of  $\beta$ -farnesene could be produced with initial glucose concentrations of 20 and 40 g/L, respectively. However, with 60 g/L of glucose, the titer value was only 2.9 g/L. Therefore, superfluous initial glucose concentration was not conducive to the accumulation of  $\beta$ -farnesene [53]. As a result, the initial glucose concentration in the fermentation medium was set to 20 g/L. In the subsequent feeding stage, the sugar restriction strategy was implemented via small amounts of glucose supplementation.

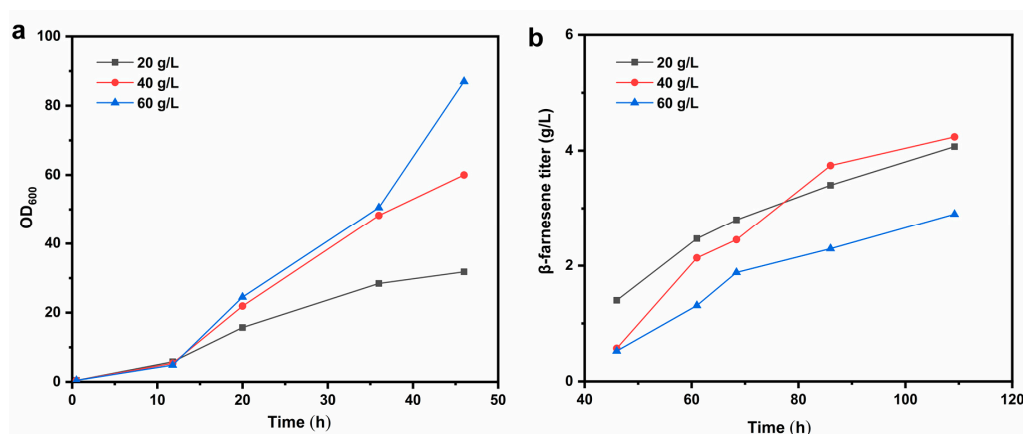


**Figure 1.** Fermentation results for the different initial glucose concentrations: (a) OD<sub>600</sub> and (b) β-farnesene titer (g/L).

### 2.1.2. Supplementary Carbon Sources and Substrate Addition Fermentation

Glucose is currently the most preferred carbon source. However, excess glucose availability can trigger the Crabtree effect [54], leading to higher growth rates of eucaryotic organisms and the accumulation of higher levels of by-products, primarily ethanol, which can influence the production of target chemicals [55]. Therefore, it is crucial to screen the appropriate carbon sources to optimize the metabolic process. To address this, we selected five carbon sources as the sole carbon source for shake-flask fermentation, including glucose [56], galactose [57], glycerol [58], ethanol [59], and sodium acetate [60]. As we can see from Figure 2a, a significant difference in β-farnesene titer was clearly observed. When the carbon sources were glucose and ethanol, the titer values of β-farnesene were as high as 1.83 and 1.86 g/L. Due to the high cost of ethanol, and its inhibition of cell growth, glucose was chosen as the supplementary carbon source.

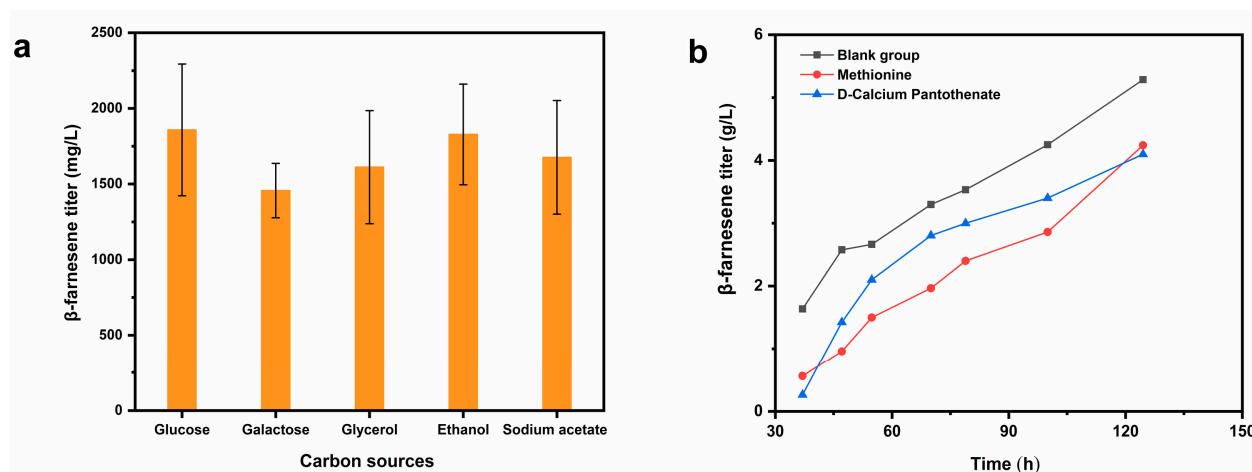


**Figure 2.** β-farnesene titer of (a) different supplementary carbon sources; (b) substrate addition fermentation.

In addition to essential elements such as carbon and nitrogen, some substrates could also be added to the medium, promoting enzyme synthesis, participating in metabolism as precursors, and reducing the accumulation of inhibitors. Methionine is an amino acid essential for protein synthesis. D-calcium pantothenate, also known as vitamin B5, serves as a precursor of coenzymes in cells. Therefore, the effects of methionine and D-calcium pantothenate on the production of β-farnesene by *S. cerevisiae* were validated. The methionine group was supplemented with 0.25 g/L of methionine based on the blank group [61]. D-calcium pantothenate group was added along with 40 mg/L of calcium D-

pantothenate based on the blank group [62]. As proposed in Figure 2b, the final production values of the blank, methionine, and D-calcium pantothenate groups were 5.29, 4.24, and 4.01 g/L, respectively. Therefore, high levels of terpenoid biosynthesis could be achieved through substrate addition such as methionine and D-calcium pantothenate, which had a negative effect on  $\beta$ -farnesene accumulation.

### 2.1.3. Fed-Batch Fermentation in a 2.5 L Bioreactor

The above fermentation scheme was carried out in a 2.5 L bioreactor, according to the optimization of technological parameters and a feeding strategy. During batch cultivation, the main growth-related parameters related to fermentation performance such as  $\beta$ -farnesene titer, glucose concentration, ethanol concentration,  $OD_{600}$ , and cell dry weight were monitored. As indicated by the exometabolism profile in Figure 3a, the final  $\beta$ -farnesene titer in the 2.5 L bioreactor reached 27.6 g/L after 203.3 h of fermentation. As shown in Figure 3b, glucose was drained after 18 h at point A, and the ethanol content simultaneously climbed to a peak of 18.53 g/L. When ethanol was consumed after 38 h at point B, the glucose and ethanol contents were maintained at a very low level, indicating that the sugar restriction strategy was realized. The peak values of  $OD_{600}$  and dry weight were 270 and 61 g/L, respectively. In summary, the yield of metabolically engineered *S. cerevisiae* BFSC0036 was stable, and the  $\beta$ -farnesene titer in the 2.5 L bioreactor was 25-fold greater than the shaking flask.

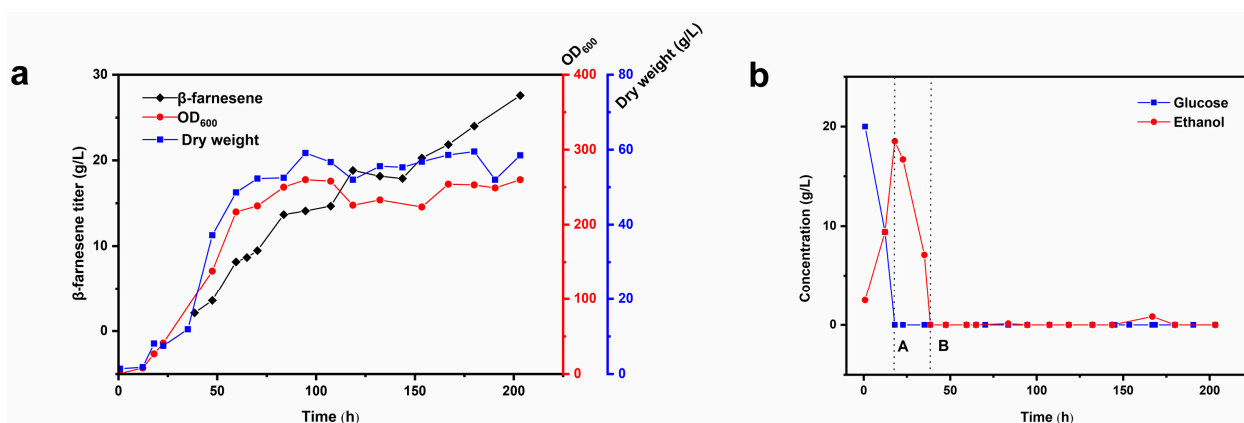


**Figure 3.** Fermentation results under optimal conditions: (a) change curves of the  $\beta$ -farnesene titer,  $OD_{600}$ , dry weight (g/L), (b) change curves of glucose concentration (g/L) and ethanol concentration (g/L).

### 2.2. Characterization and Quantification of $\beta$ -Farnesene

GC-MS was used for the identification of  $\beta$ -farnesene from microbial cell factories by comparing the mass spectrum of library retrieval. Figure 4 represented the peak with a retention time of 7.98 min, which was preliminarily confirmed as  $\beta$ -farnesene. Present in addition to the peaks with retention time of 8.18–8.65 min were a small number of by-products, including  $\alpha$ -farnesene and bisabolene. To further determine the  $\beta$ -farnesene structure, the bioproduct was subjected to NMR analysis using deuterated chloroform as the detection solvent, and the profiles are shown in Figure 5a,b [63].  $^1\text{H}$  and  $^{13}\text{C}$  NMR-chemical shifts in ppm with proton and carbon numbering are summarized in Table S1. Subsequently, FT-IR and Raman characterization was used to determine the representative chemical bonds and functional groups of  $\beta$ -farnesene. As shown in the FT-IR image in Figure 6a, the peak at  $3088\text{ cm}^{-1}$  was ascribed to the stretching vibration of  $=\text{C}-\text{H}$  for the  $\text{C}1=\text{C}2$  and  $\text{C}3=\text{C}4$  conjugated double bonds [64]. The peaks at  $1635$  and  $1670\text{ cm}^{-1}$  were attributed to the two independent double bonds of  $\text{C}7=\text{C}8$  and  $\text{C}12=\text{C}13$ , the peak at  $1596\text{ cm}^{-1}$  was assigned to the  $\text{C}1=\text{C}2$  and  $\text{C}3=\text{C}4$  conjugated double bonds, and the peaks at  $892$  and  $987\text{ cm}^{-1}$  corresponded to the  $\text{sp}^2=\text{CH}$  bending vibration of the conjugated double bond centers, respectively. As indicated by the Raman spectroscopy results in

Figure 6b, the peak at  $3008\text{ cm}^{-1}$  corresponded to the  $=\text{C}-\text{H}$  stretching of the conjugated double bond, and that at  $1423\text{ cm}^{-1}$  was attributed to the corresponding conjugated double bonds for  $\text{C}1=\text{C}2$  and  $\text{C}3=\text{C}4$  [65]. The bands at  $1634$  and  $1670\text{ cm}^{-1}$  were associated with the isolated double bonds of  $\text{C}7=\text{C}8$  and  $\text{C}12=\text{C}13$ . Therefore, the obtained NMR, FT-IR, and Raman results confirmed that the purified bioproduct was  $\beta$ -farnesene. To clarify the purity determination of the bio-privileged compound, the biological chemicals were assessed with the GC-FID system using internal standard addition with tetradecane as the internal standard at a concentration of  $900\text{ mg/L}$  and ethyl acetate as the solvent [66,67]. The standard curve preparation concentration gradient and GC spectra are shown in Table S2 and Figure S1, respectively. Finally, by substituting the integral area ratio of the sample for testing into the standard curve equation, we determined that the concentration of  $\beta$ -farnesene was 95%.

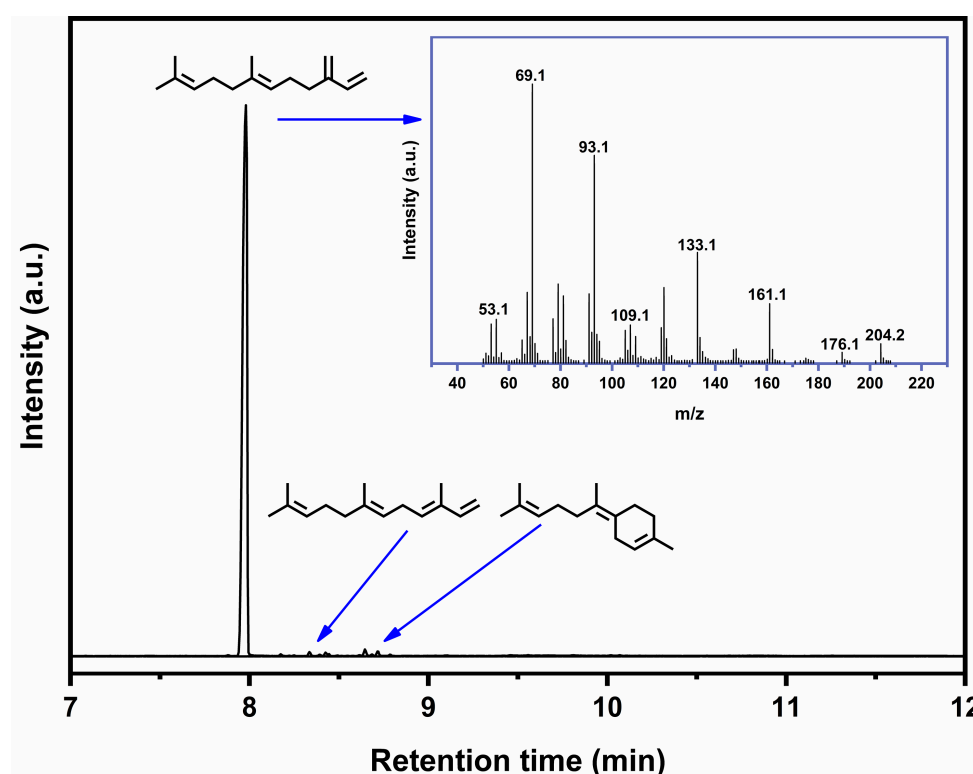


**Figure 4.** The GC-MS chromatogram and mass spectrum (insets) of  $\beta$ -farnesene from *S. cerevisiae*.

### 2.3. Palladium-Catalyzed Reductive Coupling of $\beta$ -Farnesene

To screen out the dominant organic palladium in the reaction system, the chemoactivity and stereoselectivity of seven catalysts used in this study were compared. The organopalladium catalysts assessed in the experiment consisted of  $\text{Pd}(\text{PPh}_3)_4$  [68],  $\text{Pd}(\text{OAc})_2$  [69],  $\text{Pd}(\text{acac})_2$  [70],  $\text{Pd}_2(\text{dba})_3$  [71],  $\text{Pd}(\text{cod})\text{Cl}_2$  [72],  $\text{Pd}(\text{dba})_2$  [73], and  $\text{PdCl}_2$  [74]. It is clear from Figure 7a that all catalysts exhibited high selectivity (100%) for  $\beta$ -farnesene to squalene and its isomers. However, the conversion of the  $\beta$ -farnesene substrate varied, which also indicated the necessity of catalyst selection, as illustrated in Figure 7b. The catalytic capacity of  $\text{Pd}(\text{acac})_2$  exceeded the other six organic palladium catalysts, and the conversion of  $\beta$ -farnesene reached 95% after 5 h. Therefore,  $\text{Pd}(\text{acac})_2$  was selected as the optimal catalyst and used in subsequent research for optimization of the reaction conditions.

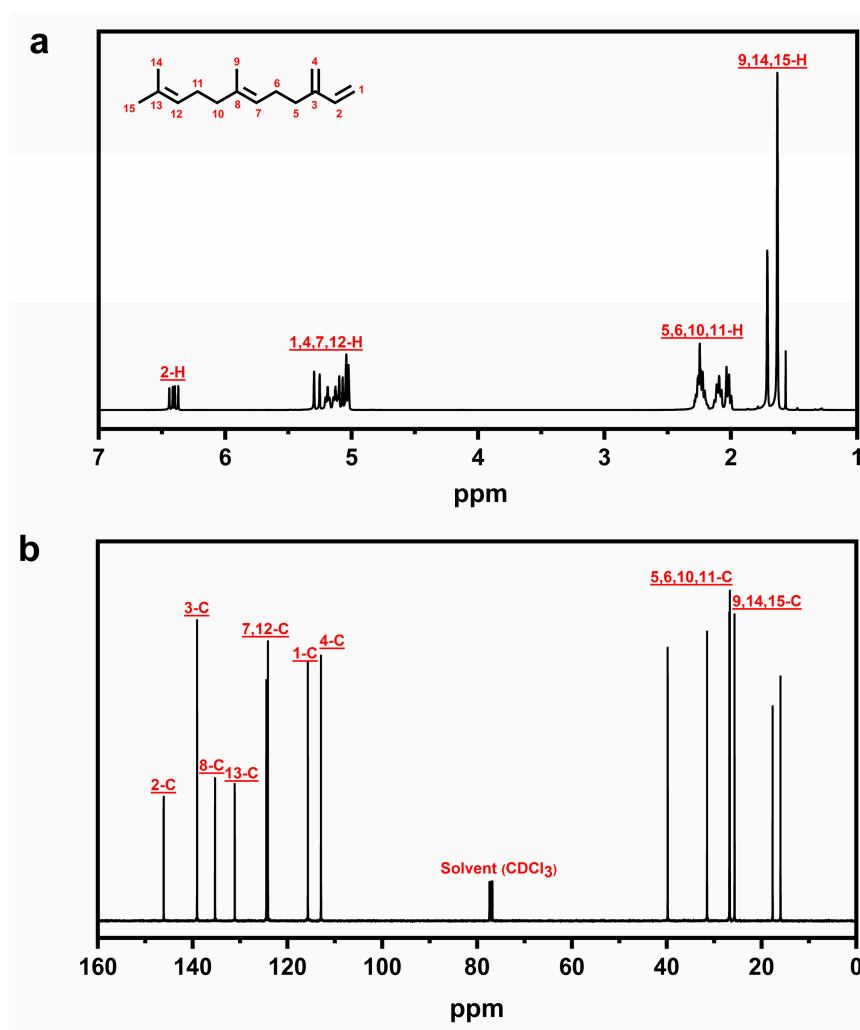


Figure 5. The NMR spectra of  $\beta$ -farnesene: (a)  $^1\text{H}$  NMR spectrum and (b)  $^{13}\text{C}$  NMR spectrum.

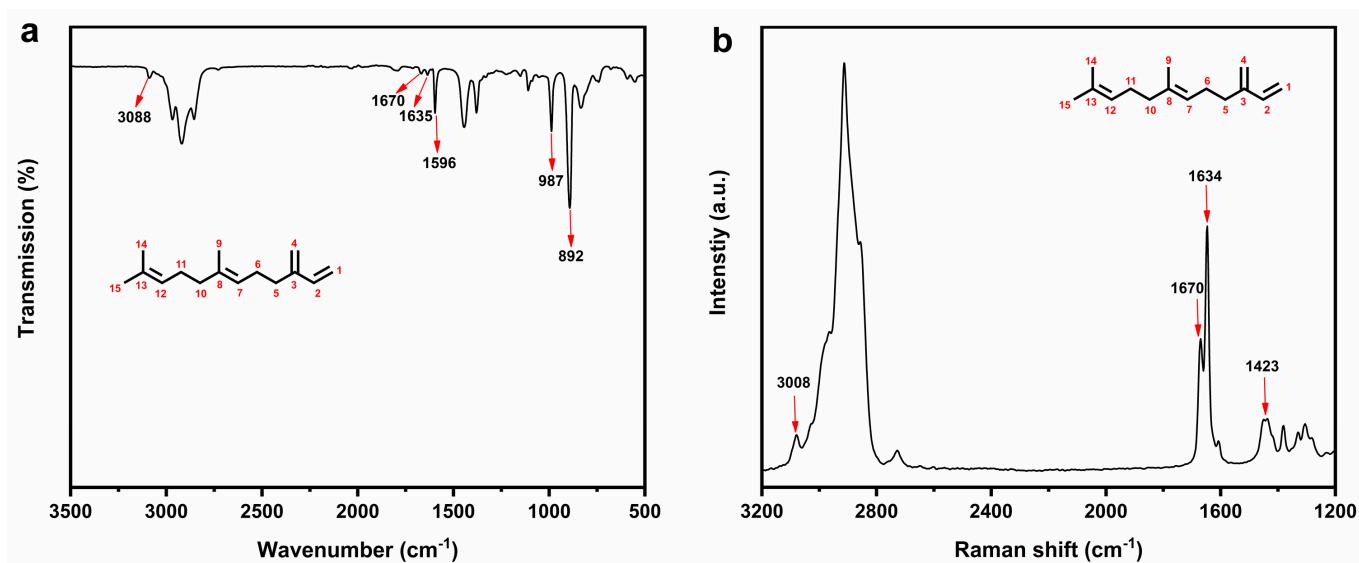
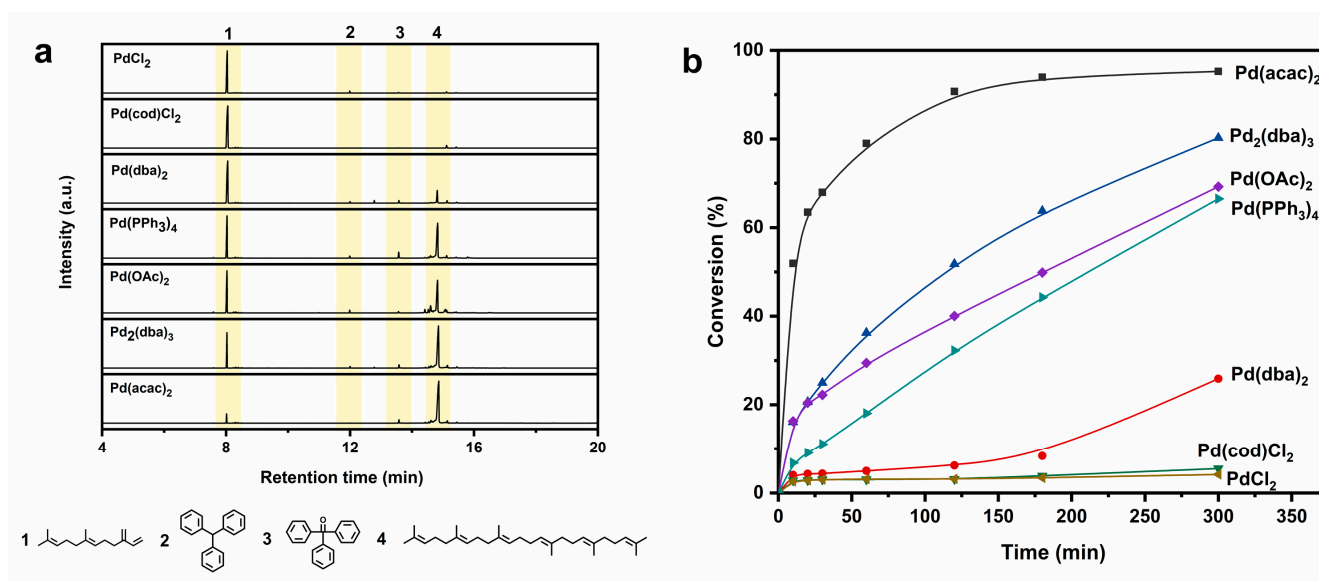


Figure 6. (a) FT-IR image and (b) Raman spectroscopy of  $\beta$ -farnesene.



**Figure 7.** Comparison of reaction results for  $\beta$ -farnesene with the seven catalysts: (a) GC-MS of the products after 5 h of reaction, (b) conversion of  $\beta$ -farnesene at 85 °C, in isopropanol substrate/catalyst = 100, and  $\text{PPh}_3/\text{catalyst} = 2.0$ ,  $C_0 = 1.0$  mol/L.

### 2.3.1. Influence of Catalyst Content on Catalytic Activity

The coupling results of  $\beta$ -farnesene when varying the catalyst content are shown in Figure 8a, using  $\text{Pd}(\text{acac})_2$  as the catalyst in the experiments. Most  $\beta$ -farnesene can be converted with substrate/catalyst ratios in the range of 50–250. Moreover, no significant difference was observed in the conversion of  $\beta$ -farnesene with different amounts of catalyst. Notably, the reaction rate with a substrate/catalyst ratio of 250 was slightly lower than with other  $\text{Pd}(\text{acac})_2$  amounts within 60 min. However, the rate gradually increased with more time, and the final conversion was as high as 98% when the reaction was carried out for 5 h. To decrease the amount of catalyst and achieve the maximum conversion of  $\beta$ -farnesene, a substrate/catalyst ratio of 250 was determined as optimal for the successive experimental exploration of the reaction conditions.

### 2.3.2. Influence of $\text{PPh}_3$ Amount on Catalytic Activity

According to the literature, a conclusion was drawn regarding the use of  $\text{PPh}_3$  as a ligand component, which was the key to cleaving the unstrained C–C bond [75]. However, phosphine has proven difficult to recycle, causing environmental and soil pollution [76]. With a general increase in environmental awareness, increasing attention has focused on dangerous drugs. Therefore, we fulfilled a series of experiments to observe the effect of different  $\text{PPh}_3/\text{catalyst}$  ratios on conversion. When the  $\text{PPh}_3/\text{catalyst}$  ratio was increased from 1.0 to 3.0, the conversion of  $\beta$ -farnesene represented significant positive progress, as proposed in Figure 8b. To achieve a balance between reducing toxic phosphine and achieving high conversion, a  $\text{PPh}_3/\text{catalyst}$  ratio of 2.0 (98% of conversion) was finally selected.

### 2.3.3. Influence of Substance Concentration on Catalytic Activity

Substrate concentration was also an arresting factor that affected the reaction rate [77]. Consequently, it was important to explore the influence of feedstock concentration. As we can see from Figure 8c, at a concentration of  $C_0 = 2.0$  mol/L, 99% of  $\beta$ -farnesene was converted to squalene without side reactions. When the coupling reaction was directed in a solvent-free microenvironment, only 10% of the raw material disappeared in 5 h. This phenomenon indicated that an appropriate substrate concentration, to a large extent, promoted the coupling reaction of  $\beta$ -farnesene.



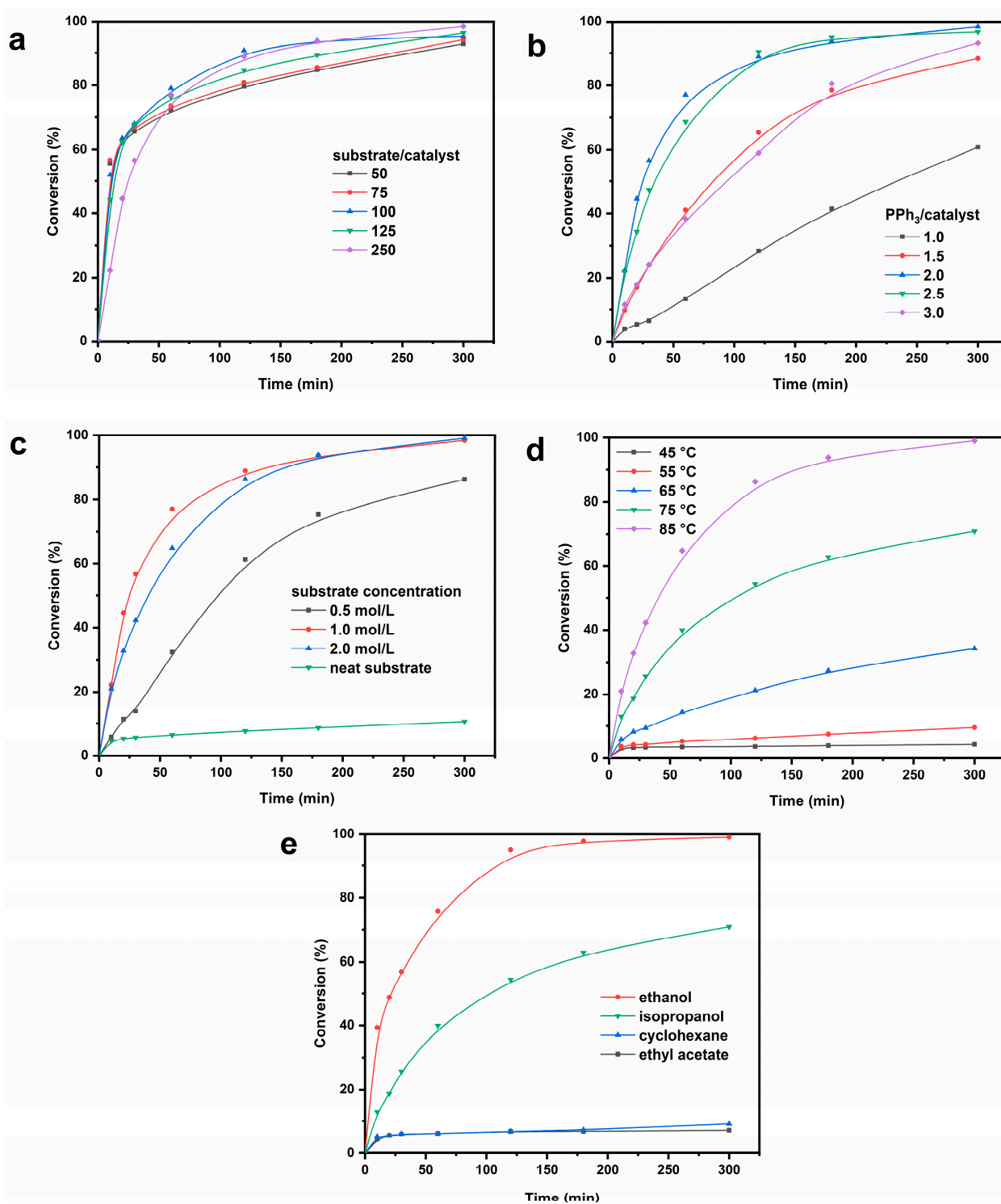


**Figure 8.** Comparison results of the optimized coupling reaction conditions of  $\beta$ -farnesene: (a–e) influence of Pd(acac)<sub>2</sub> loading, PPh<sub>3</sub> amount, substance concentration, reaction temperature, and reaction solvent on the conversion of  $\beta$ -farnesene. Reaction conditions were as follows: (a) 85 °C, in isopropanol, PPh<sub>3</sub>/catalyst = 2.0, C<sub>0</sub> = 1.0 mol/L; (b) 85 °C, in isopropanol, substrate/catalyst = 250, C<sub>0</sub> = 1.0 mol/L; (c) 85 °C, in isopropanol, substrate/catalyst = 250, PPh<sub>3</sub>/catalyst = 2.0; (d) in isopropanol, substrate/catalyst = 250, PPh<sub>3</sub>/catalyst = 2.0, C<sub>0</sub> = 2.0 mol/L; (e) 75 °C, substrate/catalyst = 250, PPh<sub>3</sub>/catalyst = 2.0, C<sub>0</sub> = 2.0 mol/L.

### 2.3.4. Influence of Reaction Temperature on Catalytic Activity

The effect of reaction temperature was established in rapid sequence. In these experiments, additional reaction parameter variables were immobilized with  $C_0 = 2.0$  mol/L,  $PPh_3/\text{catalyst} = 2.0$ , and  $\text{substrate}/\text{catalyst} = 250$ . As expected, a significant positive effect of up-regulated reaction temperature was achieved and the best result was obtained at  $85^\circ\text{C}$  (99% of conversion, Figure 8d). In the temperature range of  $65\text{--}85^\circ\text{C}$ , the conversion rate increased significantly. Therefore, the reductive coupling reaction of  $\beta$ -farnesene was sensitive to temperature, and the conversion could be improved by increasing the reaction temperature.

### 2.3.5. Influence of Reaction Solvent on Catalytic Activity

The beneficial effect of the solvent was clearly observed in the contrast experiments of substrate concentration. From a practical standpoint, the use of non-toxic, stabilized, and inexpensive solvents is the goal of large-scale industrial production [78]. Therefore, we selected four reaction solvents including isopropanol [79], ethanol [80], cyclohexane [81], and ethyl acetate [82] (at  $75^\circ\text{C}$ ,  $\text{substrate}/\text{catalyst} = 250$ ,  $PPh_3/\text{catalyst} = 2.0$ ,  $C_0 = 2.0$  mol/L, Figure 8e). Compared to the other three solvents, 95% conversion of  $\beta$ -farnesene was achieved in the ethanol medium after only 2 h. In addition, 99% of  $\beta$ -farnesene was transformed at  $75^\circ\text{C}$  when the reaction was applied for 5 h, which was comparable to the results presented in the isopropanol environment at  $85^\circ\text{C}$ . This result further confirmed the superiority of ethanol as an alternative solvent for the coupling reaction of  $\beta$ -farnesene. In addition, as can be seen from Figure 9, reduction coupling in the existing literature has problems of high catalyst dosage and low selectivity, resulting in increased cost and low yield of target products [83,84]. In this study, palladium-catalyzed farnesene coupling to squalene showed excellent reactivity and stereoselectivity, which enriched the production path of squalene.

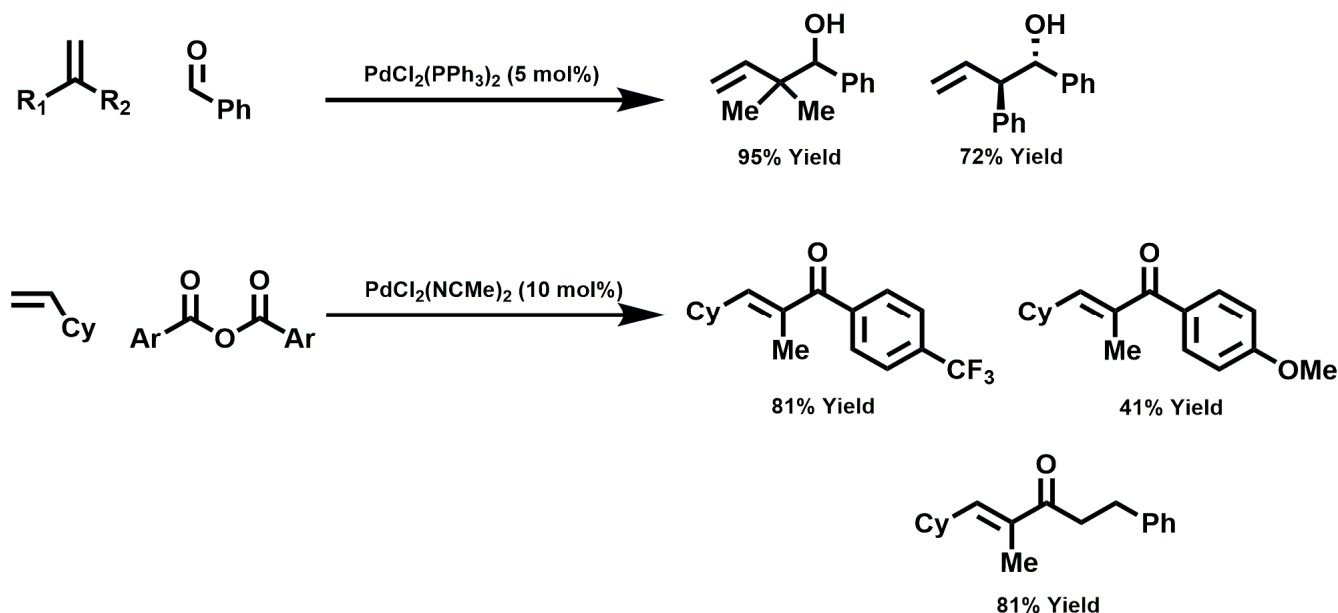


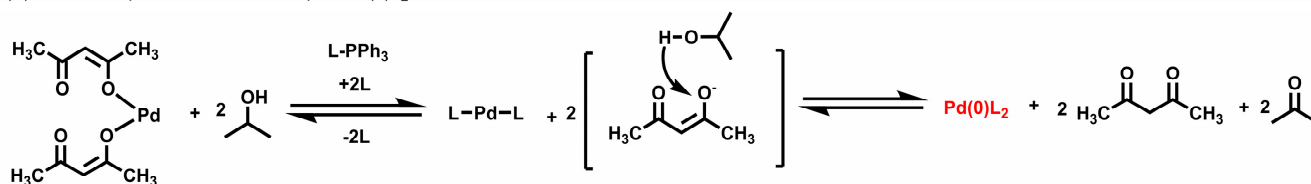
**Figure 9.** Palladium-catalyzed allene-aldehyde reductive coupling.

### 2.4. Reaction Mechanism for Reductive Coupling of $\beta$ -Farnesene

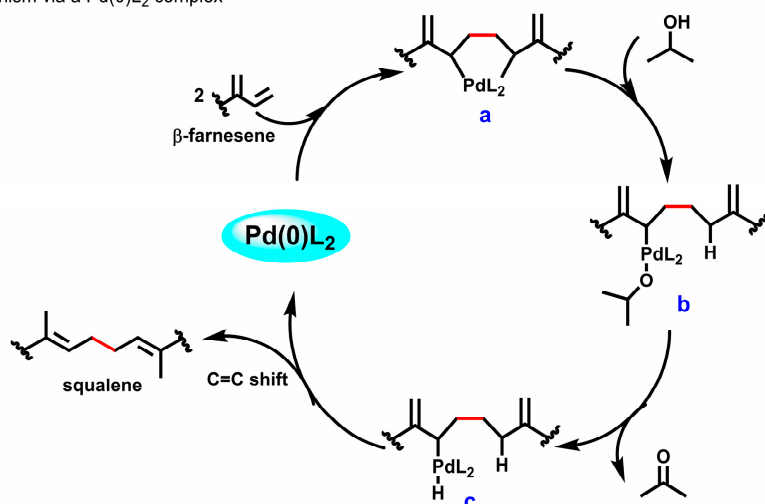
Based on these aforementioned results and the reported information that the cyclometallation of palladium and diene could be easily formed, a plausible mechanism was depicted in Scheme 2 [85–87]. As we can see from Scheme 2A, when  $Pd(\text{acac})_2$  and  $PPh_3$  were dispersed in an isopropanol medium, isopropanol acted as the hydrogen transfer agent to promote the formation of  $Pd(0)L_2$  species. Subsequently, the catalytic coupling of

$\beta$ -farnesene to squalene was completed in the presence of  $\text{Pd}(0)\text{L}_2$  as shown in Scheme 2B. Initially, the activate palladium  $\text{Pd}(0)\text{L}_2$  coordinated to two molecules of  $\beta$ -farnesene, forming the palladium-cycle structure **a** and initiating the coupling reaction. Next, the transition state **a** was protonated in the microenvironment of abundant isopropanol to generate a ring-opening intermediate **b**. Further, intermediate **b** underwent  $\beta$ -H elimination to produce intermediate **c**. Lastly, reductive elimination of intermediate **c** terminated the chain, followed by shift of  $\text{C}=\text{C}$  bonds, delivering the desired product squalene and regenerating the active palladium species  $\text{Pd}(0)\text{L}_2$ . Similarly, ethanol medium also followed this reaction mechanism. However, ethyl acetate and cyclohexane struggled to afford the required hydride source in this reaction path to obtain  $\text{Pd}(0)\text{L}_2$  system, which was consistent with the low conversion of  $\beta$ -farnesene.

(A) Formation process of active complex  $\text{Pd}(0)\text{L}_2$



(B) Proposed mechanism via a  $\text{Pd}(0)\text{L}_2$  complex



**Scheme 2.** Reaction mechanism for reductive coupling of  $\beta$ -farnesene to squalene.

### 2.5. Separation and Purification of the Coupling Reaction Products

After concentration, the coupling reaction products in the downstream chemical transformations consisted of a dark-brown fluid, which could not be used in end-use applications for fuel additives or fine chemicals. In this case, the squalene component was column purified with 90% recovery using silica gel chromatography and detected via TLC and GC-MS [88]. From Figure 10, we can see that triphenylphosphine, triphenylphosphine oxyphosphate, and palladium catalysts, as well as other compositions, remained in the column, resulting in a colorless, transparent, oily liquid. The MS spectrum of squalene is shown in Figure S2. In addition, the purified product was characterized via NMR confirmation, and the chemical shifts of the  $^1\text{H}$  and  $^{13}\text{C}$  NMR spectrums were obtained (Figure 11 and Table S3). After spectrogram analysis, we verified that the collected products were squalene in peak 7 and trace isomers in peak 6 and 8.

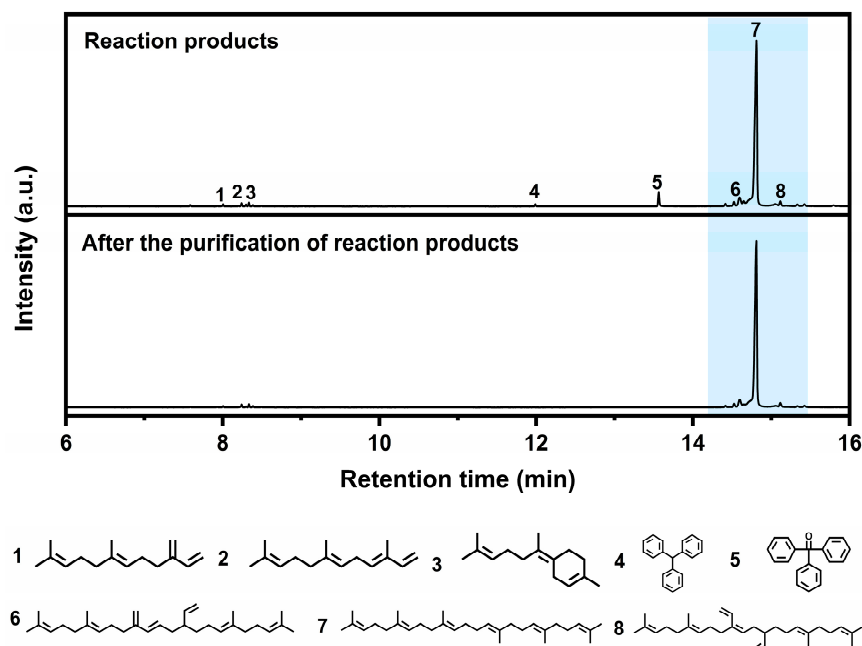


Figure 10. The GC-MS chromatogram of the crude and purified products.

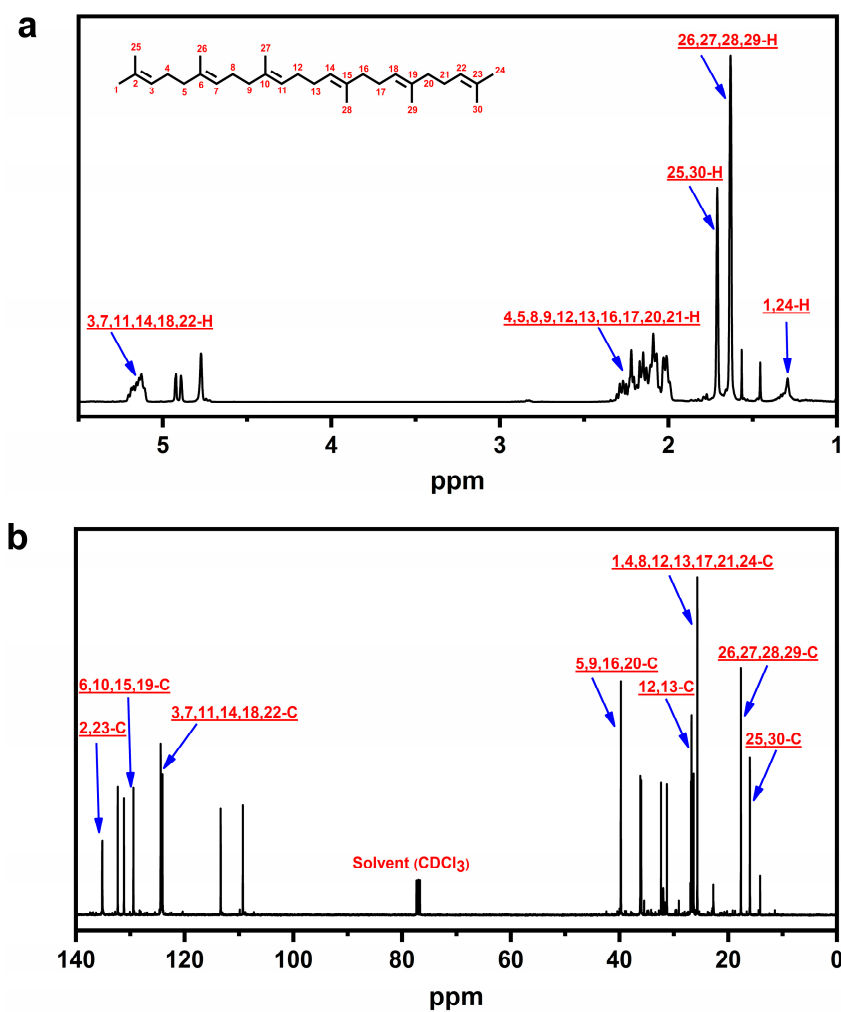


Figure 11. NMR spectra of squalene: (a)  $^1\text{H}$  NMR spectrum and (b)  $^{13}\text{C}$  NMR spectrum.

### 3. Experimental Section

#### 3.1. Materials and Chemicals

Glucose ( $C_6H_{12}O_6 \cdot H_2O$ ), poly  $\alpha$ -olefin, and yeast extract were procured from AOB Biotech, Inc. (Beijing, China). Peptone and agar powder were purchased from Sigma-Aldrich Trading Co., Ltd. (Beijing, China). Homogeneous palladium catalysts, including  $Pd(PPh_3)_4$  (CAS: 14221-01-3),  $Pd(OAc)_2$  (CAS: 3375-31-3),  $Pd(acac)_2$  (CAS: 14024-61-4),  $Pd_2(dba)_3$  (CAS: 51364-51-3),  $Pd(cod)Cl_2$  (CAS: 12107-56-1),  $Pd(dba)_2$  (CAS: 32005-36-0), and  $PdCl_2$  (CAS: 7647-10-1) were obtained from Shanghai Aladdin Reagent Co., Ltd., (Shanghai, China), and the molecular structures are listed in Figure S3. Triphenylphosphine was supplied by Shanghai Damas-beta Co., Ltd. (Shanghai, China). Isopropyl alcohol, ethyl acetate, ethanol, cyclohexane, n-heptane, dodecane, and tetradecane were purchased from Honeywell Inc. (Nanjing, China). Silica gel (200–300 mesh) used for column chromatographic purification was obtained from Shanghai Aladdin Reagent Co., Ltd. (Shanghai, China). All chemicals and solvents were used directly in the experiments without further purification.

In this work, a  $\beta$ -farnesene-producing strain BFSC0036 was constructed by transforming BFSC0001 as the starting strain with plasmid pYES2-FS, which carried the corresponding farnesene synthetase gene. The specific modification pathway is shown in Figure S4 and the methods were conducted according to Zhao et al. [89]. Yeast Peptone Dextrose was used for the seed medium, which contained 10 g/L of yeast extract, 20 g/L of glucose, and 20 g/L of peptone. Agar plate as the solid medium was supplemented with 15 g/L of agar based on the Yeast Peptone Dextrose medium. The synthetic medium contained 15 g/L of  $(NH_4)_2SO_4$ , 9 g/L of  $KH_2PO_4$ , 6.25 g/L of  $MgSO_4 \cdot 7H_2O$ , 20 g/L of glucose, 12 mL/L of vitamin solution, 10 mL/L of trace metal solution, and 0.5 M 100 mL/L of succinic acid solution. The compositions of the vitamin and trace metal solutions are described in the materials and methods section in the Supporting Information. The strains in 70% (v/v) glycerol solution were frozen at an ultra-low temperature for long-term storage.

#### 3.2. Product Analysis

The organic products were characterized using gas chromatography and mass spectrometry (GC-MS, Shimadzu QP2010 SE W). The instrument was fitted with an autosampler and an HP-5 capillary column, where 10  $\mu$ L of the concentrated sample was dissolved in 1 mL of solvent (HPLC grade), filtered with a filtration membrane, and then directly used for component analysis. Helium was used as the carrier gas, and the split ratio was set to 100 at a pressure of 149.5 kPa. The column temperature program was set to an initial temperature of 50  $^\circ$ C for 1 min, followed by a ramp rate of 20  $^\circ$ C/min to 300  $^\circ$ C for 10 min. The resolution of the peaks in the spectrogram was determined via automatic library retrieval, such as NIST 17 and NIST 17s.

Quantitative analysis of the obtained products was performed using gas chromatography (GC, Shimadzu 2010 pro). The GC system was equipped with a flame ionization detector (FID) and an HP-5MS column. Nitrogen was used as the carrier gas, and the split ratio was set to 100 at a pressure of 149.5 kPa. A total of 10 mL of fermentation broth was centrifuged at  $8000 \times g$  rpm for 10 min, and the supernatant was the desired organic solution. The mixed liquid containing 20  $\mu$ L of organic solution and 180  $\mu$ L of internal standard (1 g of tetradecane in 1000 mL of ethyl acetate) was analyzed to calculate the content of  $\beta$ -farnesene. The column temperature program was started at 100  $^\circ$ C for 1 min, followed by a ramp rate of 20  $^\circ$ C/min to 230  $^\circ$ C for 2 min, and increased up to 315  $^\circ$ C at a ramp rate of 30  $^\circ$ C/min for 20 min. The detection temperature was 320  $^\circ$ C. The tetradecane concentration was approximately 900 mg/L, similar to the concentration in the standard curve. The sample was equivalent to 10-fold dilution, and the  $\beta$ -farnesene concentration was calculated using the standard curve equation.

Fourier transform infrared (FT-IR) spectroscopy analysis can be used to determine the molecular structure of organic compounds through the characteristic peak positions and peak shapes of the different functional groups. In this study, we utilized a Thermo Fisher

Nicolet Is5 Fourier infrared spectrometer (the United States) for analysis. The sample was assessed in attenuated total reflection mode at room temperature and positioned in the light path for scanning.

The Raman patterns were recorded with a Thermo Fisher Dxr2xi spectrometer with a 532 nm laser source in the spectral range of 50–3400  $\text{cm}^{-1}$ . The sample was placed on a glass slide and scanned using an InGaN laser.

The purified components were investigated via nuclear magnetic resonance (NMR) spectroscopy using a Bruker 400 MHz nuclear magnetic resonance instrument. For component analysis, 10 mg of the sample was dissolved in 0.5 mL of deuterated chloroform. After the specimen was scanned multiple times, the hydrogen spectrum and carbon spectrum data of the substance were obtained to determine the structure of the substance.

### 3.3. Fed-Batch Fermentation in a 2.5 L Bioreactor

The detailed procedures for preparing the preculture and conducting shake flask cultivations are presented in the Supporting Information Materials and Methods Section. Cultivation of the  $\beta$ -farnesene-producing strain was performed in a 2.5 L bioreactor (Xcubio twin) with 40% loading, which contained 800 mL of synthetic medium, 100 mL of secondary seed solution, and 100 mL of poly  $\alpha$ -olefin extraction agent (biphasic medium fermentation). Because poly  $\alpha$ -olefin had a boiling point above 500  $^{\circ}\text{C}$  and  $\beta$ -farnesene at 273  $^{\circ}\text{C}$ , facile distillation could be used to separate the two. The fermentation process was maintained at 30  $^{\circ}\text{C}$ , with an agitation speed ranging from 200 to 700 rpm. The percentage of dissolved oxygen (DO) was controlled at 40% and the pH was adjusted to 5.0 using 10 M  $\text{NH}_4\text{OH}$  with a starting  $\text{OD}_{600}$  of 0.1. The airflow rate was set to 1 vvm. All parameters were adjusted via a control cabinet equipped with the bioreactor. Samples were obtained at specific times to measure parameters of variation in cell growth.

### 3.4. Separation and Purification Steps of $\beta$ -Farnesene from the Biphasic Medium

The fermentation broth contained the solid phase of the bacterial cells, consisting of the aqueous phase of the medium and the organic phase of the extractant. Therefore, it was necessary to first separate the organic phase from the fermentation broth, and then extract  $\beta$ -farnesene from the organic phase. To separate the  $\beta$ -farnesene solution from the three phases, the mixture was centrifuged at  $4500 \times g$  rpm for 20 min. Subsequently, to purify the  $\beta$ -farnesene component from the organic phase, the organic liquid was collected via a centrifugal extractor and then concentrated through a rotary evaporator under the conditions of 3 mbar and 190  $^{\circ}\text{C}$ . The resulting light phase samples from decompressing distillation process were tested qualitatively and quantitatively using GC-MS and GC, respectively.

### 3.5. Palladium-Catalyzed Reductive Coupling of $\beta$ -Farnesene

In a typical experiment, 0.15 mmol of  $\text{Pd}(\text{acac})_2$ , 0.30 mmol of  $\text{PPh}_3$ , and 13.4 mL of isopropanol (substrate/catalyst = 100,  $\text{PPh}_3$ /catalyst = 2.0,  $C_0 = 1.0$  mol/L) were placed in a dry three-necked flask. The flask was secured and purged under nitrogen flow for 20 min. Subsequently, 15 mmol of  $\beta$ -farnesene was added dropwise to the flask with a syringe, and the system was purged with nitrogen for several minutes. The reaction system was carried out on an IKA heated magnetic agitator at 85  $^{\circ}\text{C}$ . Samples were taken at set time intervals and the reaction mixture was analyzed using GC and GC-MS.

### 3.6. Column Purification of the Coupling Reaction Products

The coupling reaction products were purified via column chromatography on silica gel in a glass column, using a mixture of petroleum ether and ethyl acetate (10:1 gradient) as the eluent. Then, 1.0 g of silica gel and 5.0 g of crude product in ethanol solution were added to a 100 mL eggplant-shaped flask. The solid–liquid mixture was completely evaporated out of the organic solvent, and the sample was evenly spread over the dry silica powder surface. Subsequently, the remaining silica powder was coated on top of the 30.0 g of silica column. The column was thoroughly washed with petroleum ether and eluted with

petroleum ether-ethyl acetate, and the components of the dripped eluent were monitored using thin-layer chromatography (TLC) and GC-MS. The collected fractions were rotary evaporated to remove the organic solution.

#### 4. Conclusions

This study presented the efficient conversion of cellulosic biomass into performance-advantaged chemicals and fuels using hybrid processes with microbial fermentation technology and olefin reductive coupling. Under optimal culture conditions, glucose derived from the hydrolysis of cellulose was used as a carbon source with an initial concentration of 20 g/L and no added substrates, achieving a total of 27.6 g/L of  $\beta$ -farnesene using fed-batch fermentation in a 2.5 L bioreactor. Biobased  $\beta$ -farnesene was transformed to squalene with desirable properties, with a yield of 99% over the Pd(acac)<sub>2</sub> catalyst in an ethanol solvent and at a temperature of 75 °C. Furthermore, the active catalytic species Pd(0)L<sub>2</sub> was generated to typically initiate the reductive coupling of  $\beta$ -farnesene under the condition of low-carbon alcohol (ethanol or isopropanol) as the reductant reagent. The flexibility of the bioprocess coupled with the molecular stereochemistry specificity allowed for metabolic engineering in yeasts or bacteria, with more suitable cultivation conditions. This advancement in biobased  $\beta$ -farnesene coupling may promote the biorenewable energy development of C30 squalene and its derivatives to alternate petrochemical counterparts, creating new compounds in the market. From a sustainability perspective, our findings provided a blueprint for the diversification of products from biomass in a tandem reaction with biocatalysis and chemocatalysis, combining the unparalleled selectivity of the former with the robust reactivity of the latter.

**Supplementary Materials:** The following supporting information can be downloaded at: <https://www.mdpi.com/article/10.3390/catal13111392/s1>, Solution composition, Preparation of preculture and shake flask cultivations; Table S1. Biobased  $\beta$ -farnesene of the <sup>1</sup>H and <sup>13</sup>C NMR-chemical shifts; Table S2. Concentration gradient of standard curve; Figure S1. GC chromatogram of  $\beta$ -farnesene using internal standard method (retention time 5.102 min: tetradecane; retention time 5.545 min:  $\beta$ -farnesene); Figure S2. Mass spectrum of the purified squalene product; Table S3. Purified squalene of the <sup>1</sup>H and <sup>13</sup>C NMR-chemical shifts; Figure S3. Molecular structure of homogeneous palladium catalysts; Figure S4. Strain transformation route.

**Author Contributions:** C.W.: investigation, conceptualization, methodology, formal analysis, visualization, validation, writing—original draft, writing—review and editing. K.T.: investigation, conceptualization, methodology, formal analysis, visualization, validation, resources. X.G.: investigation, data curation, supervision, writing—review and editing. Y.F.: methodology, funding acquisition, project administration, supervision. All authors have read and agreed to the published version of the manuscript.

**Funding:** This study was supported by National Key Research and Development Program of China (No. 2021YFC2103703).

**Data Availability Statement:** Data will be made available on request.

**Conflicts of Interest:** The authors declare no conflict of interest.

#### References

1. Liu, Y.; Cruz-Morales, P.; Zargar, A.; Belcher, M.S.; Pang, B.; Englund, E.; Dan, Q.; Yin, K.; Keasling, J.D. Biofuels for a sustainable future. *Cell* **2021**, *184*, 1636–1647. [[CrossRef](#)]
2. Albers, S.C.; Berklund, A.M.; Graff, G.D. The rise and fall of innovation in biofuels. *Nat. Biotechnol.* **2016**, *34*, 814–821. [[CrossRef](#)]
3. Ripa, M.; Cadillo-Benalcazar, J.J.; Giampietro, M. Cutting through the biofuel confusion: A conceptual framework to check the feasibility, viability and desirability of biofuels. *Energy Strategy Rev.* **2021**, *35*, 100642. [[CrossRef](#)]
4. Joshi, G.; Pandey, J.K.; Rana, S.; Rawat, D.S. Challenges and opportunities for the application of biofuel. *Renew. Sustain. Energy Rev.* **2017**, *79*, 850–866. [[CrossRef](#)]
5. Kumaniaev, I.; Navare, K.; Crespo Mendes, N.; Placet, V.; Van Acker, K.; Samec, J.S.M. Conversion of birch bark to biofuels. *Green Chem.* **2020**, *22*, 2255–2263. [[CrossRef](#)]

6. Sikarwar, V.S.; Zhao, M.; Fennell, P.S.; Shah, N.; Anthony, E.J. Progress in biofuel production from gasification. *Prog. Energy Combust. Sci.* **2017**, *61*, 189–248. [[CrossRef](#)]
7. Bryant, N.D.; Pu, Y.; Tschaplinski, T.J.; Tuskan, G.A.; Muchero, W.; Kalluri, U.C.; Yoo, C.G.; Ragauskas, A.J. Transgenic Poplar Designed for Biofuels. *Trends Plant Sci.* **2020**, *25*, 881–896. [[CrossRef](#)] [[PubMed](#)]
8. Stafford, W.; De Lange, W.; Nahman, A.; Chunilall, V.; Lekha, P.; Andrew, J.; Johakimu, J.; Sithole, B.; Trotter, D. Forestry biorefineries. *Renew. Energy* **2020**, *154*, 461–475. [[CrossRef](#)]
9. Bang, J.; Ahn, J.H.; Lee, J.A.; Hwang, C.H.; Kim, G.B.; Lee, J.; Lee, S.Y. Synthetic Formatotrophs for One-Carbon Biorefinery. *Adv. Sci.* **2021**, *8*, 2100199. [[CrossRef](#)] [[PubMed](#)]
10. Rinaldi, R. A Tandem for Lignin-First Biorefinery. *Joule* **2017**, *1*, 427–428. [[CrossRef](#)]
11. Lari, G.M.; Pastore, G.; Haus, M.; Ding, Y.; Papadokonstantakis, S.; Mondelli, C.; Pérez-Ramírez, J. Environmental and economical perspectives of a glycerol biorefinery. *Energy Environ. Sci.* **2018**, *11*, 1012–1029. [[CrossRef](#)]
12. Branco-Vieira, M.; San Martin, S.; Agurto, C.; Freitas, M.A.V.; Martins, A.A.; Mata, T.M.; Caetano, N.S. Biotechnological potential of *Phaeodactylum tricornutum* for biorefinery processes. *Fuel* **2020**, *268*, 117357. [[CrossRef](#)]
13. Liao, P.; Hemmerlin, A.; Bach, T.J.; Chye, M.-L. The potential of the mevalonate pathway for enhanced isoprenoid production. *Biotechnol. Adv.* **2016**, *34*, 697–713. [[CrossRef](#)]
14. Laskin, A.; Laskin, J.; Nizkorodov, S.A. Chemistry of Atmospheric Brown Carbon. *Chem. Rev.* **2015**, *115*, 4335–4382. [[CrossRef](#)] [[PubMed](#)]
15. Brown, A.J.; Chua, N.K.; Yan, N. The shape of human squalene epoxidase expands the arsenal against cancer. *Nat. Commun.* **2019**, *10*, 888. [[CrossRef](#)] [[PubMed](#)]
16. Pollier, J.; Vancaester, E.; Kuzhiumparambil, U.; Vickers, C.E.; Vandepoele, K.; Goossens, A.; Fabris, M. A widespread alternative squalene epoxidase participates in eukaryote steroid biosynthesis. *Nat. Microbiol.* **2019**, *4*, 226–233. [[CrossRef](#)]
17. Liu, Y.; Wang, Z.; Cui, Z.; Qi, Q.; Hou, J. Progress and perspectives for microbial production of farnesene. *Bioresour. Technol.* **2022**, *347*, 126682. [[CrossRef](#)]
18. Briou, B.; Ameduri, B.; Boutevin, B. Trends in the Diels–Alder reaction in polymer chemistry. *Chem. Soc. Rev.* **2021**, *50*, 11055–11097. [[CrossRef](#)]
19. Strong, P.J.; Xie, S.; Clarke, W.P. Methane as a resource: Can the methanotrophs add value? *Environ. Sci. Technol.* **2015**, *49*, 4001–4018. [[CrossRef](#)]
20. Orzolek, B.J.; Rahman, M.A.; Iovine, P.M. Synthesis of Biorenewable Starch–Farnesene Amphiphilic Conjugates via Transesterification of Terpene-Derived Diels–Alder Adducts. *ACS Sustain. Chem. Eng.* **2018**, *6*, 13562–13569. [[CrossRef](#)]
21. Ding, J.; You, S.; Ba, W.; Zhang, H.; Chang, H.; Qi, W.; Su, R.; He, Z. Bifunctional utilization of whey powder as a substrate and inducer for beta-farnesene production in an engineered *Escherichia coli*. *Bioresour. Technol.* **2021**, *341*, 125739. [[CrossRef](#)]
22. Wang, J.; Chen, N.; Bian, G.; Mu, X.; Du, N.; Wang, W.; Ma, C.G.; Fu, S.; Huang, B.; Liu, T.; et al. Solar-Driven Overproduction of Biofuels in Microorganisms. *Angew. Chem. Int. Ed.* **2022**, *61*, e202207132. [[CrossRef](#)] [[PubMed](#)]
23. Meadows, A.L.; Hawkins, K.M.; Tsegaye, Y.; Antipov, E.; Kim, Y.; Raetz, L.; Dahl, R.H.; Tai, A.; Mahatdejkul-Meadows, T.; Xu, L.; et al. Rewriting yeast central carbon metabolism for industrial isoprenoid production. *Nature* **2016**, *537*, 694–697. [[CrossRef](#)] [[PubMed](#)]
24. Lv, J.; Wang, Y.; Zhang, C.; You, S.; Qi, W.; Su, R.; He, Z. Highly efficient production of FAMES and  $\beta$ -farnesene from a two-stage biotransformation of waste cooking oils. *Energy Convers. Manag.* **2019**, *199*, 112001. [[CrossRef](#)]
25. Tippmann, S.; Nielsen, J.; Khoomrung, S. Improved quantification of farnesene during microbial production from *Saccharomyces cerevisiae* in two-liquid-phase fermentations. *Talanta* **2016**, *146*, 100–106. [[CrossRef](#)]
26. Tippmann, S.; Anfelt, J.; David, F.; Rand, J.M.; Siewers, V.; Uhlen, M.; Nielsen, J.; Hudson, E.P. Affibody Scaffolds Improve Sesquiterpene Production in *Saccharomyces cerevisiae*. *ACS Synth. Biol.* **2017**, *6*, 19–28. [[CrossRef](#)]
27. Tippmann, S.; Scalcinati, G.; Siewers, V.; Nielsen, J. Production of farnesene and santalene by *Saccharomyces cerevisiae* using fed-batch cultivations with RQ-controlled feed. *Biotechnol. Bioeng.* **2016**, *113*, 72–81. [[CrossRef](#)]
28. Han, J.Y.; Song, J.M.; Seo, S.H.; Wang, C.; Lee, S.G.; Lee, H.; Kim, S.W.; Choi, E.S. Ty1-fused protein-body formation for spatial organization of metabolic pathways in *Saccharomyces cerevisiae*. *Biotechnol. Bioeng.* **2018**, *115*, 694–704. [[CrossRef](#)]
29. Liu, C.-L.; Xue, K.; Yang, Y.; Liu, X.; Li, Y.; Lee, T.S.; Bai, Z.; Tan, T. Metabolic engineering strategies for sesquiterpene production in microorganism. *Crit. Rev. Biotechnol.* **2022**, *42*, 73–92. [[CrossRef](#)]
30. Carvalho, L.C.; Oliveira, A.L.S.; Carsanba, E.; Pintado, M.; Oliveira, C. Phenolic compounds modulation in  $\beta$ -farnesene fed-batch fermentation using sugarcane syrup as feedstock. *Ind. Crops Prod.* **2022**, *188*, 115721. [[CrossRef](#)]
31. Tippmann, S.; Ferreira, R.; Siewers, V.; Nielsen, J.; Chen, Y. Effects of acetoacetyl-CoA synthase expression on production of farnesene in *Saccharomyces cerevisiae*. *J. Ind. Microbiol. Biotechnol.* **2017**, *44*, 911–922. [[CrossRef](#)] [[PubMed](#)]
32. Sandoval, C.M.; Ayson, M.; Moss, N.; Lieu, B.; Jackson, P.; Gaucher, S.P.; Horning, T.; Dahl, R.H.; Denery, J.R.; Abbott, D.A.; et al. Use of pantothenate as a metabolic switch increases the genetic stability of farnesene producing *Saccharomyces cerevisiae*. *Metab. Eng.* **2014**, *25*, 215–226. [[CrossRef](#)] [[PubMed](#)]
33. Schwartz-Narbonne, H.; Wang, C.; Zhou, S.; Abbatt, J.P.D.; Faust, J. Heterogeneous Chlorination of Squalene and Oleic Acid. *Environ. Sci. Technol.* **2019**, *53*, 1217–1224. [[CrossRef](#)] [[PubMed](#)]
34. Chua, N.K.; Coates, H.W.; Brown, A.J. Squalene monooxygenase: A journey to the heart of cholesterol synthesis. *Prog. Lipid Res.* **2020**, *79*, 101033. [[CrossRef](#)]



35. Park, J.; Kang, D.H.; Woo, H.M. Microbial Bioprocess for Extracellular Squalene Production and Formulation of Nanoemulsions. *ACS Sustain. Chem. Eng.* **2021**, *9*, 14263–14276. [[CrossRef](#)]
36. Kimura, K.; Shiraiishi, K.; Kondo, T.; Nakamura, J.; Fujitani, T. Cracking of squalene into isoprene as chemical utilization of algae oil. *Green Chem.* **2020**, *22*, 3083–3087. [[CrossRef](#)]
37. Cheng, P.; Okada, S.; Zhou, C.; Chen, P.; Huo, S.; Li, K.; Addy, M.; Yan, X.; Ruan, R.R. High-value chemicals from *Botryococcus braunii* and their current applications—A review. *Bioresour. Technol.* **2019**, *291*, 121911. [[CrossRef](#)]
38. Thapa, H.R.; Naik, M.T.; Okada, S.; Takada, K.; Molnar, I.; Xu, Y.; Devarenne, T.P. A squalene synthase-like enzyme initiates production of tetraterpenoid hydrocarbons in *Botryococcus braunii* Race L. *Nat. Commun.* **2016**, *7*, 11198. [[CrossRef](#)]
39. Xu, W.; Yao, J.; Liu, L.; Ma, X.; Li, W.; Sun, X.; Wang, Y. Improving squalene production by enhancing the NADPH/NADP<sup>+</sup> ratio, modifying the isoprenoid-feeding module and blocking the menaquinone pathway in *Escherichia coli*. *Biotechnol. Biofuels* **2019**, *12*, 68. [[CrossRef](#)]
40. Patel, A.; Bettiga, M.; Rova, U.; Christakopoulos, P.; Matsakas, L. Microbial genetic engineering approach to replace shark livering for squalene. *Trends Biotechnol.* **2022**, *40*, 1261–1273. [[CrossRef](#)]
41. Moula Ali, A.M.; Prodpran, T.; Benjakul, S. Effect of squalene rich fraction from shark liver on mechanical, barrier and thermal properties of fish (*Probarbus jullieni*) skin gelatin film. *Food Hydrocoll.* **2019**, *96*, 123–133. [[CrossRef](#)]
42. Tenllado, D.; Reglero, G.; Torres, C.F. A combined procedure of supercritical fluid extraction and molecular distillation for the purification of alkylglycerols from shark liver oil. *Sep. Purif. Technol.* **2011**, *83*, 74–81. [[CrossRef](#)]
43. Fisher, K.J.; Kinsey, R.; Mohamath, R.; Phan, T.; Liang, H.; Orr, M.T.; Lykins, W.R.; Guderian, J.A.; Bakken, J.; Argilla, D.; et al. Semi-synthetic terpenoids with differential adjuvant properties as sustainable replacements for shark squalene in vaccine emulsions. *NPJ Vaccines* **2023**, *8*, 14. [[CrossRef](#)]
44. Zhou, X.; Zhang, G.; Huang, R.; Huang, H. Palladium-Catalyzed Allyl-Allyl Reductive Coupling of Allylamines or Allylic Alcohols with H<sub>2</sub> as Sole Reductant. *Org. Lett.* **2021**, *23*, 365–369. [[CrossRef](#)] [[PubMed](#)]
45. Holmes, M.; Schwartz, L.A.; Krische, M.J. Intermolecular Metal-Catalyzed Reductive Coupling of Dienes, Allenes, and Enynes with Carbonyl Compounds and Imines. *Chem. Rev.* **2018**, *118*, 6026–6052. [[CrossRef](#)] [[PubMed](#)]
46. Wu, K.-Q.; Li, H.; Zhou, A.; Yang, W.-R.; Yin, Q. Palladium-Catalyzed Chemo- and Regioselective C–H Bond Functionalization of Phenols with 1,3-Dienes. *J. Org. Chem.* **2023**, *88*, 2599–2604. [[CrossRef](#)]
47. Zargari, N.; de Prevoisin, G.; Kim, Y.; Kaneshiro, K.; Runburg, R.; Park, J.; LaCroix, K.; Narain, R.; Lee, B.D.; Lee, J.H.; et al. Hydroalkenylation: Palladium catalyzed co-dimerization of unactivated alkenes. *Tetrahedron Lett.* **2016**, *57*, 815–818. [[CrossRef](#)]
48. Cai, G.; Ding, M.; Wu, Q.; Jiang, H.L. Encapsulating soluble active species into hollow crystalline porous capsules beyond integration of homogeneous and heterogeneous catalysis. *Natl. Sci. Rev.* **2020**, *7*, 37–45. [[CrossRef](#)]
49. Lang, R.; Li, T.; Matsumura, D.; Miao, S.; Ren, Y.; Cui, Y.T.; Tan, Y.; Qiao, B.; Li, L.; Wang, A.; et al. Hydroformylation of Olefins by a Rhodium Single-Atom Catalyst with Activity Comparable to RhCl(PPh<sub>3</sub>)<sub>3</sub>. *Angew. Chem. Int. Ed.* **2016**, *55*, 16054–16058. [[CrossRef](#)]
50. Li, H.; Chen, G.; Duchesne, P.N.; Zhang, P.; Dai, Y.; Yang, H.; Wu, B.; Liu, S.; Xu, C.; Zheng, N. A nanoparticulate polyacetylene-supported Pd(II) catalyst combining the advantages of homogeneous and heterogeneous catalysts. *Chin. J. Catal.* **2015**, *36*, 1560–1572. [[CrossRef](#)]
51. Zhang, H.-H.; Tang, M.; Zhao, J.-J.; Song, C.; Yu, S. Enantioselective Reductive Homocoupling of Allylic Acetates Enabled by Dual Photoredox/Palladium Catalysis: Access to C2-Symmetrical 1,5-Dienes. *J. Am. Chem. Soc.* **2021**, *143*, 12836–12846. [[CrossRef](#)] [[PubMed](#)]
52. Liu, F.; Tian, Y.; Ding, Y.; Li, Z. The use of fermentation liquid of wastewater primary sedimentation sludge as supplemental carbon source for denitrification based on enhanced anaerobic fermentation. *Bioresour. Technol.* **2016**, *219*, 6–13. [[CrossRef](#)] [[PubMed](#)]
53. Mahmoud, M.; Torres, C.I.; Rittmann, B.E. Changes in Glucose Fermentation Pathways as a Response to the Free Ammonia Concentration in Microbial Electrolysis Cells. *Environ. Sci. Technol.* **2017**, *51*, 13461–13470. [[CrossRef](#)] [[PubMed](#)]
54. Darshi, M.; Tumova, J.; Saliba, A.; Kim, J.; Baek, J.; Pennathur, S.; Sharma, K. Crabtree effect in kidney proximal tubule cells via late-stage glycolytic intermediates. *iScience* **2023**, *26*, 106462. [[CrossRef](#)]
55. Malina, C.; Yu, R.; Bjorkeröth, J.; Kerkhoven, E.J.; Nielsen, J. Adaptations in metabolism and protein translation give rise to the Crabtree effect in yeast. *Proc. Natl. Acad. Sci. USA* **2021**, *118*, e2112836118. [[CrossRef](#)]
56. Liu, X.; Lin, L.; Xu, X.; Zhang, H.; Wu, L.; Zhu, P.; Li, S.; Xu, H. Two-step economical welan gum production by *Sphingomonas* sp. HT-1 from sugar industrial by-products. *Carbohydr. Polym.* **2018**, *181*, 412–418. [[CrossRef](#)]
57. He, F.; Qin, S.; Yang, Z.; Bai, X.; Suo, Y.; Wang, J. Butyric acid production from spent coffee grounds by engineered *Clostridium tyrobutyricum* overexpressing galactose catabolism genes. *Bioresour. Technol.* **2020**, *304*, 122977. [[CrossRef](#)]
58. Xiberras, J.; Klein, M.; Nevoigt, E. Glycerol as a substrate for *Saccharomyces cerevisiae* based bioprocesses—Knowledge gaps regarding the central carbon catabolism of this ‘non-fermentable’ carbon source. *Biotechnol. Adv.* **2019**, *37*, 107378. [[CrossRef](#)]
59. Policastro, G.; Giugliano, M.; Luongo, V.; Napolitano, R.; Fabbri, M. Carbon catabolite repression occurrence in photo fermentation of ethanol-rich substrates. *J. Environ. Manag.* **2021**, *297*, 113371. [[CrossRef](#)]
60. Zhang, Y.; Wang, X.C.; Cheng, Z.; Li, Y.; Tang, J. Effects of additional fermented food wastes on nitrogen removal enhancement and sludge characteristics in a sequential batch reactor for wastewater treatment. *Environ. Sci. Pollut. Res. Int.* **2016**, *23*, 12890–12899. [[CrossRef](#)]

61. Paddon, C.J.; Westfall, P.J.; Pitera, D.J.; Benjamin, K.; Fisher, K.; McPhee, D.; Leavell, M.D.; Tai, A.; Main, A.; Eng, D.; et al. High-level semi-synthetic production of the potent antimalarial artemisinin. *Nature* **2013**, *496*, 528–532. [[CrossRef](#)]
62. Webb, M.E.; Smith, A.G.; Abell, C. Biosynthesis of pantothenate. *Nat. Prod. Rep.* **2004**, *21*, 695–721. [[CrossRef](#)] [[PubMed](#)]
63. Szafranek, B.; Chrapkowska, K.; Pawińska, M.; Szafranek, J. Analysis of Leaf Surface Sesquiterpenes in Potato Varieties. *J. Agric. Food Chem.* **2005**, *53*, 2817–2822. [[CrossRef](#)] [[PubMed](#)]
64. Svatoš, A.; Attygalle, A.B. Characterization of Vinyl-Substituted, Carbon-Carbon Double Bonds by GC/FT-IR Analysis. *Anal. Chem.* **1997**, *69*, 1827–1836. [[CrossRef](#)] [[PubMed](#)]
65. Zhuang, Y.; Ren, Z.; Jiang, L.; Zhang, J.; Wang, H.; Zhang, G. Raman and FTIR spectroscopic studies on two hydroxylated tung oils (HTO) bearing conjugated double bonds. *Spectrochim. Acta A Mol. Biomol. Spectrosc.* **2018**, *199*, 146–152. [[CrossRef](#)] [[PubMed](#)]
66. Watanabe, T.; Kato, K.; Tsunoda, K.-i.; Maeda, T. Metrological effectiveness of an analytical method for volatile organic compounds standard materials using post-column reaction GC/FID system. *Anal. Chim. Acta* **2008**, *619*, 26–29. [[CrossRef](#)]
67. Niculescu, R.; Năstase, M.; Clenci, A. On the determination of the distillation curve of fatty acid methyl esters by gas chromatography. *Fuel* **2022**, *314*, 123143. [[CrossRef](#)]
68. Gao, J.; Wang, W.; Zhang, S.; Xiao, S.; Zhan, C.; Yang, M.; Lu, X.; You, W. Distinction between PTB7-Th samples prepared from Pd(PPh<sub>3</sub>)<sub>4</sub> and Pd<sub>2</sub>(dba)<sub>3</sub>/P(o-tol)<sub>3</sub> catalysed stille coupling polymerization and the resultant photovoltaic performance. *J. Mater. Chem. A* **2018**, *6*, 179–188. [[CrossRef](#)]
69. Shao, Q.; Wu, K.; Zhuang, Z.; Qian, S.; Yu, J.-Q. From Pd(OAc)<sub>2</sub> to Chiral Catalysts: The Discovery and Development of Bifunctional Mono-N-Protected Amino Acid Ligands for Diverse C–H Functionalization Reactions. *Acc. Chem. Res.* **2020**, *53*, 833–851. [[CrossRef](#)]
70. Petters, L.; Burger, S.; Kronawitter, S.; Drees, M.; Kieslich, G. Linear negative thermal expansion in Pd(acac)<sub>2</sub>. *CrystEngComm* **2021**, *23*, 5425–5429. [[CrossRef](#)]
71. Janusson, E.; Zijlstra, H.S.; Nguyen, P.P.T.; MacGillivray, L.; Martelino, J.; McIndoe, J.S. Real-time analysis of Pd<sub>2</sub>(dba)<sub>3</sub> activation by phosphine ligands. *Chem. Commun.* **2017**, *53*, 854–856. [[CrossRef](#)]
72. Mikhel, I.S.; Gavrilov, K.N.; Polosukhin, A.I.; Rebrov, A.I. Reactions of chiral phosphoramidites with complexes Pd(COD)Cl<sub>2</sub> and Pt(COD)Cl<sub>2</sub>. *Russ. Chem. Bull.* **1998**, *47*, 1585–1588. [[CrossRef](#)]
73. Cong, M.; Fan, Y.; Raimundo, J.-M.; Tang, J.; Peng, L. Pd(dba)<sub>2</sub> vs Pd<sub>2</sub>(dba)<sub>3</sub>: An in-Depth Comparison of Catalytic Reactivity and Mechanism via Mixed-Ligand Promoted C–N and C–S Coupling Reactions. *Org. Lett.* **2014**, *16*, 4074–4077. [[CrossRef](#)] [[PubMed](#)]
74. Mondal, M.; Bora, U. An efficient protocol for palladium-catalyzed ligand-free Suzuki–Miyaura coupling in water. *Green Chem.* **2012**, *14*, 1873–1876. [[CrossRef](#)]
75. Chen, P.-P.; Wipf, P.; Houk, K.N. How mono- and diphosphine ligands alter regioselectivity of the Rh-catalyzed annulative cleavage of bicyclo[1.1.0]butanes. *Nat. Commun.* **2022**, *13*, 7292. [[CrossRef](#)]
76. Krachko, T.; Bispinghoff, M.; Tondreau, A.M.; Stein, D.; Baker, M.; Ehlers, A.W.; Slootweg, J.C.; Grützmacher, H. Facile Phenylphosphinidene Transfer Reactions from Carbene–Phosphinidene Zinc Complexes. *Angew. Chem. Int. Ed.* **2017**, *56*, 7948–7951. [[CrossRef](#)] [[PubMed](#)]
77. Swansborough-Aston, W.A.; Soltan, A.; Coulson, B.; Pratt, A.; Chechik, V.; Douthwaite, R.E. Efficient photoelectrochemical Kolbe C–C coupling at BiVO<sub>4</sub> electrodes under visible light irradiation. *Green Chem.* **2023**, *25*, 1067–1077. [[CrossRef](#)]
78. Bisz, E.; Szostak, M. 2-Methyltetrahydrofuran: A Green Solvent for Iron-Catalyzed Cross-Coupling Reactions. *ChemSusChem* **2018**, *11*, 1290–1294. [[CrossRef](#)]
79. Camp, J.E.; Dunsford, J.J.; Cannons, E.P.; Restorick, W.J.; Gadzhieva, A.; Fay, M.W.; Smith, R.J. Glucose-Derived Palladium(0) Nanoparticles as in Situ-Formed Catalysts for Suzuki–Miyaura Cross-Coupling Reactions in Isopropanol. *ACS Sustain. Chem. Eng.* **2014**, *2*, 500–505. [[CrossRef](#)]
80. Corulli, C.J.; Groover, E.A.; Attelah, J.D.; Miller, C.B.; Penland, B.B. Rational design of peptides for biomimetic palladium nanoparticle catalysis with Suzuki and Heck coupling in ethanol. *Colloid Interface Sci. Commun.* **2023**, *54*, 100708. [[CrossRef](#)]
81. Datta, A.; Ebert, K.; Plenio, H. Nanofiltration for Homogeneous Catalysis Separation: Soluble Polymer-Supported Palladium Catalysts for Heck, Sonogashira, and Suzuki Coupling of Aryl Halides. *Organometallics* **2003**, *22*, 4685–4691. [[CrossRef](#)]
82. Ricordi, V.G.; Freitas, C.S.; Perin, G.; Lenardão, E.J.; Jacob, R.G.; Savegnago, L.; Alves, D. Glycerol as a recyclable solvent for copper-catalyzed cross-coupling reactions of diaryl diselenides with aryl boronic acids. *Green Chem.* **2012**, *14*, 1030–1034. [[CrossRef](#)]
83. Chang, H.-M.; Cheng, C.-H. Highly Regioselective and Stereoselective Allylation of Aldehydes via Palladium-Catalyzed in Situ Hydrostannylation of Allenes. *Org. Lett.* **2000**, *2*, 3439–3442. [[CrossRef](#)] [[PubMed](#)]
84. Fujihara, T.; Tatsumi, K.; Terao, J.; Tsuji, Y. Palladium-Catalyzed Formal Hydroacylation of Allenes Employing Acid Chlorides and Hydrosilanes. *Org. Lett.* **2013**, *15*, 2286–2289. [[CrossRef](#)] [[PubMed](#)]
85. Yao, W.-W.; Li, R.; Li, J.-F.; Sun, J.; Ye, M. NHC ligand-enabled Ni-catalyzed reductive coupling of alkynes and imines using isopropanol as a reductant. *Green Chem.* **2019**, *21*, 2240–2244. [[CrossRef](#)]
86. Gu, Z.-Y.; Li, W.-D.; Li, Y.-L.; Cui, K.; Xia, J.-B. Selective Reductive Coupling of Vinyl Azaarenes and Alkynes via Photoredox Cobalt Dual Catalysis. *Angew. Chem. Int. Ed.* **2023**, *62*, e202213281. [[CrossRef](#)]
87. Marion, N.; Nolan, S.P. Well-Defined N-Heterocyclic Carbenes–Palladium(II) Precatalysts for Cross-Coupling Reactions. *Acc. Chem. Res.* **2008**, *41*, 1440–1449. [[CrossRef](#)]

88. Kumar, S.S.; Manasa, V.; Tumaney, A.W.; Bettadaiah, K.B.; Chaudhari, S.R.; Giridhar, P. Chemical composition, nutraceuticals characterization, NMR confirmation of squalene and antioxidant activities of *Basella rubra* L. seed oil. *RSC Adv.* **2020**, *10*, 31863–31873. [[CrossRef](#)]
89. Zhao, L.; Xu, L.; Westfall, P.; Main, A. Methods of developing terpene synthase variants. KR Patent KR20130110226A, 1 February 2012.

**Disclaimer/Publisher’s Note:** The statements, opinions and data contained in all publications are solely those of the individual author(s) and contributor(s) and not of MDPI and/or the editor(s). MDPI and/or the editor(s) disclaim responsibility for any injury to people or property resulting from any ideas, methods, instructions or products referred to in the content.